(24) Wang, M.; Ledford, E. B., Jr.; Marshall, A. G. FACSS XIV Annual Meeting, Detroit, MI October 1987; Abstract No. 43.
(25) Comisarow, M. B. *J. Chem. Phys.* **1978**, *69*, 4097-4104.
(26) Comisarow, M. B. In *Ion Cyclotron Resonance Spectrometry II*; Springer-Verlag: Berlin, 1982; pp 484-513.
(27) Grosshans, P. B.; Marshall, A. G. *Collected Abstracts*; American Society for Mass Spectrometry 37th Annual Conference on Mass Spectrometry & Allied Topics, 1989; American Society for Mass Spectrometry: East Lansing, MI, 1989; pp 1232-1233.
(28) Rempel, D. L.; Huang, S. K.; Gross, M. L. *Int. J. Mass Spectrom. Ion Processes* **1986**, *70*, 163-184.
(29) Huang, S. K.; Rempel, D. L.; Gross, M. L. *Int. J. Mass Spectrom. Ion Processes* **1986**, *72*, 15-31.
(30) Allemann, M.; Kofel, P.; Kellerhals, Hp.; Wanczek, K.-P. *Int. J. Mass Spectrom. Ion Processes* **1987**, *75*, 47-54.
(31) Van der Hart, W. J.; Van De Guchte, W. J. *Int. J. Mass Spectrom. Ion Processes* **1988**, *82*, 17-31.
(32) Dunbar, R. C. *Int. J. Mass Spectrom. Ion Processes* **1984**, *56*, 1-9.
(33) Chen, L.; Cottrell, C. E.; Marshall, A. G. *Chemom. Intell. Lab. Syst.* **1986** *1*, 51-58.
(34) Liang, Z.; Marshall, A. G. *Anal. Chem.* **1990**, *62*, 70-75.
(35) Sommer, H.; Thomas, H. A.; Hipple, J. A. *Phys. Rev.* **1951**, *82*, 697-702.
(36) Hanson, C. D.; Castro, M. E.; Kerley, E. L.; Russell, D. H. *Anal. Chem.*, following paper in this issue.
(37) Wang, M.; Marshall, A. G. *Anal. Chem.* **1989**, *61*, 1288-1293.
(38) Beauchamp, J. L.; Armstrong, J. T. *Rev. Sci. Instrum.* **1969**, *40*, 123-128.
(39) Kerley, E. L.; Russell, D. H. *Anal. Chem.* **1989**, *61*, 53-57.
(40) Hanson, C. D.; Kerley, E. L.; Russell, D. H. *Anal. Chem.* **1989**, *61*, 83-85.
(41) Marshall, A. G.; Wang, T.-C. L.; Ricca, T. L. *J. Am. Chem. Soc.* **1985**, *107*, 7893-7897.

RECEIVED for review August 7, 1989. Accepted November 6, 1989. This work was supported by grants (to A.G.M.) from the National Science Foundation (CHE-87-21498), the U.S. Public Health Service (NIH GM-31683), and The Ohio State University.

Field-Corrected Ion Cell for Ion Cyclotron Resonance

Curtiss D. Hanson

Department of Chemistry, University of Northern Iowa, Cedar Falls, Iowa 50614

Mauro E. Castro, Eric L. Kerley, and David H. Russell*

Department of Chemistry, Texas A&M University, College Station, Texas 77843

The basis for mass analysis by Fourier transform ion cyclotron resonance (FT-ICR) is the motion of ions in a homogeneous magnetic field. Electric fields are used in FT-ICR to modify ion motion (i.e., trapping and excitation fields). Ion interaction with inhomogeneous radio frequency and direct current (dc) electric fields complicates the ion motion and leads to loss of both resolution and sensitivity. Modifying the geometry of the FT-ICR cell to produce uniform ion acceleration and homogeneous dc trapping fields results in simplified frequency measurements and studies of ion-molecule reactions.

INTRODUCTION

Mass analysis by Fourier transform ion cyclotron resonance (FT-ICR) is achieved by relating the frequency of an ion's periodic orbital motion (in a homogeneous magnetic field) to the mass-to-charge (m/z) ratio (*1-4*). The fundamental consideration of mass analysis by FT-ICR is that an ion's orbital frequency is *solely* dependent upon its m/z ratio. The ICR ion cell is designed to trap ions in an electrostatic well, and acceleration of the ions is accomplished by applying a variable frequency radio frequency (rf) electric field. Consequently, the ions experience forces due to the electric fields and the materials used to construct the ICR cell have some degree of magnetic properties which result in regions of magnetic inhomogeneities. The additional forces acting on the ions (the applied electric fields or inhomogeneous magnetic fields) result in aberrations of the ion motion which must be accounted for by using correction factors or calibration tables (*5, 6*). Although early work showed that the effects of magnetic inhomogeneities can be ignored for single-cell experiments (*7, 8*), more recent work clearly demonstrates the importance of cell materials for experiments involving ion transportation through small orifices (i.e., two-section cell experiments and injection from an external ion source) (*9*). Furthermore, ion motion resulting from an applied electrostatic trapping field has been shown to cause both frequency shifts and side bands (*10, 11*). On the basis of these considerations, both construction materials and cell geometries must be carefully selected to ensure predictable signal response. Corrections for the cyclotron frequency in a trapped ICR cell are difficult to derive because frequency perturbations caused by inhomogeneous $\mathbf{E} \times \mathbf{B}$ fields are dependent upon the geometry of the ion cell (*12*). Although analytical treatment of the equations for ion motion have been derived for specific cell geometries, the resulting frequency corrections are difficult to use for ions either having large spatial distributions or existing in field boundaries where the $\mathbf{E} \times \mathbf{B}$ fields are ill-defined.

In a pure homogeneous $\mathbf{E} \times \mathbf{B}$ field, the dc electric trapping field only affects the motion of the ions along the Z axis. Conversely, in an inhomogeneous $\mathbf{E} \times \mathbf{B}$ field, the electrostatic trapping field creates a net force perpendicular to the ion motion which alters the frequency of the ion's orbit. These effects are illustrated by evaluating the forces acting on an ion cycloiding about the central axis of a symmetric trapping field where the radial force of the electric field is constant. Equation 1 shows the contributions of the radial magnetic and electric field forces acting on an ion of mass m and charge q in an $\mathbf{E} \times \mathbf{B}$ field

$$mv_{\perp}^2/r + qE \sin \phi = qv_{\perp}B \qquad (1)$$

where $v_{\perp}$ is the scalar component of the ion velocity perpendicular to the magnetic field lines (in the X-Y plane). Because the *total* outward radial force is the sum of the centrifugal and electric field forces, the radial force due to the applied dc electric field ($E \sin \phi$) shifts the ion's cyclotron frequency to lower values. The frequency difference between an ion experiencing a radial electric field and the natural cyclotron frequency increases with the redirection of the

0003-2700/90/0362-0520$02.50/0

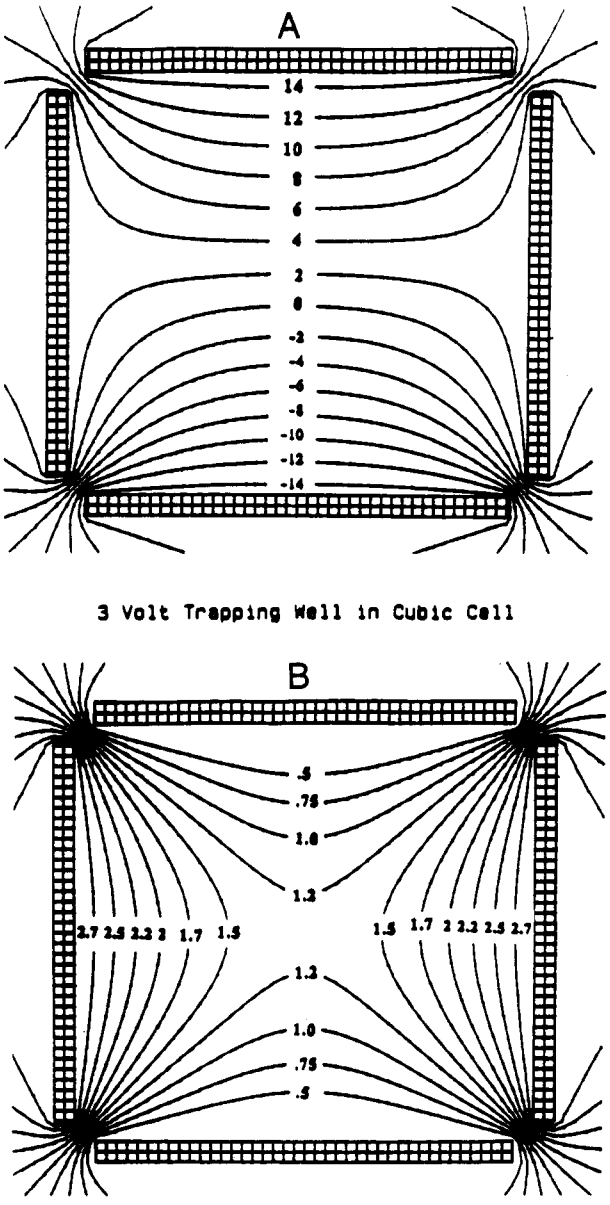

Figure 1. Computer simulation plots of the electric equipotential field lines generated by (A) an rf electric field and (B) a dc trapping field in a cubic FT-ICR cell.

electric field (E) into the X–Y plane (where ϕ is the angle between the dc electric field vector and the magnetic field lines). Therefore, the angular velocity of an ion in an inhomogeneous $\mathbf{E} \times \mathbf{B}$ field is not solely dependent upon the m/z ratio; it is also dependent upon the magnitude of the dc electric field (eq 2). In addition, the perpendicular component of the

$$\omega_{ion} = v_\perp / r = q/mv_\perp(v_\perp B - E \sin \phi) \qquad (2)$$

applied trapping field causes a drift of the center of the orbital motion. The resulting magnetron motion causes sidebands flanking the main peak.

The trapped ion cell most commonly used for ICR consists of six electrically isolated plates arranged in cubical geometry (*13*, *14*). Although this cell design was originally used to approximate a quadrupolar electric field, the six flat plates cause significant redirection of the electric fields used for trapping and excitation. Figure 1 contains plots of the field lines resulting from an rf excitation electric field (A) and the dc trapping field (B). The rf excitation field is contoured by the excite and receive plates and the dc trapping field contains lines of force which have components in the X–Y and Z directions. Because the perpendicular component of the electric

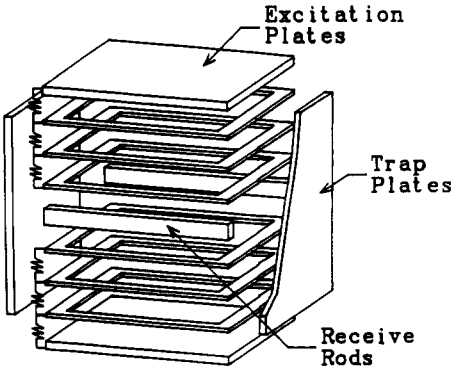

Figure 2. Field-corrected ion cell utilizes shimming rings similar to the omegatron to ensure a uniform rf excitation. The uniform excitation is achieved by linearly decreasing the magnitude of the voltages applied to the rings.

field is radially inhomogeneous, the frequency of an ion in a cubic ICR cell varies with cyclotron radius (i.e., ion position in the X–Y plane) (*15*). Ion motion is also affected by the quadratic potential gradient along the Z axis; specifically, ions formed in the electrostatic well created by the trapping plates are accelerated along the Z axis (*16*). Ions that are trapped in the cell have a distribution of kinetic energies along the Z axis ranging between the translational energy of the neutral prior to ionization and the potential of the trapping well. Furthermore, the redirection of the excitation field causes an axial component of the excitation field resulting in Z-axis excitation (*17–19*).

To eliminate the problems associated with $\mathbf{E} \times \mathbf{B}$ fields, cell designs have been introduced which reduce or eliminate the electric field within the detection region of the FT-ICR cell (*17*, *20–23*). The ideal ion cell for FT-ICR would be constructed of plates having infinite dimensions. The infinite plates would eliminate the redirection of the electric field lines caused by multiple electrode interaction. Although it is impossible to construct such a cell, uniform field lines can be produced by incorporating shimming electrodes. The omegatron ion cell used for mass analysis by Sommer, Thomas, and Hipple (*24–26*) incorporated "guard rings" to shim the applied rf electric field. This design ensured uniform excitation fields at the boundaries of a finite ion cell. A uniform rf excitation field is achieved by linearly decreasing the magnitude of the voltages applied to the rings. However, the omegatron cell design is not compatible with an FT-ICR detection scheme. The field-corrected ICR cell (Figure 2) is a modified omegatron cell which is compatible with FT-ICR ion detection. Uniform electric fields (both dc and rf) are produced by placing guard rings between the excitation plates and in front of the trapping plates. Figure 3 contains plots of the rf and dc electric fields produced by the field-corrected ICR cell. Note that the rf excitation field is uniform throughout the full cell dimensions and that the trapping well is shielded eliminating frequency shifts during detection (*23*).

The obstacle to using the field-corrected cell for FT-ICR is the design of the electrode used to receive the signal. In order to ensure homogeneous rf electric fields, guard rings are used to shim the electric fields in both the X–Z and the Y–Z planes. Placement of guard rings in front of the signal receive electrodes shields the induced image current and causes signal loss. With receive electrodes inside the guard ring assembly, there is no shielding effect and signal loss. An ion cell utilizing single wire or small rod detection electrodes combined with guard rings ensures homogeneous electric fields and minimizes signal loss. The purpose of this paper is to evaluate the effects of (i) reducing the surface area of the receive electrodes (i.e., receive rods) and (ii) the use of guard rings on frequency measurements by FT-ICR.

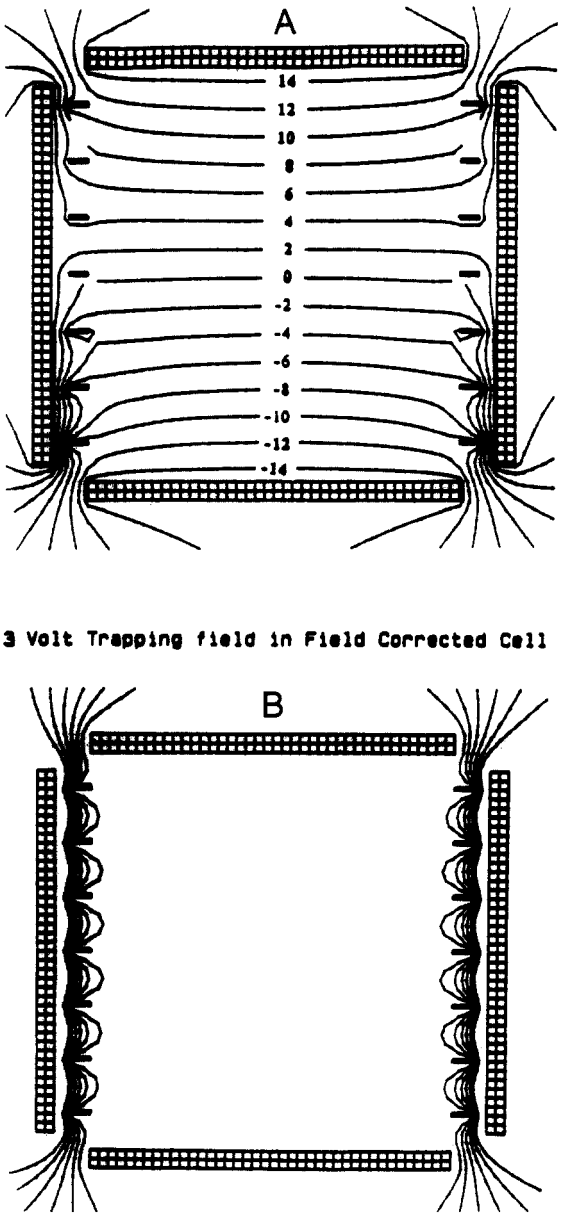

Figure 3. Computer simulation plots of the electric equipotential field lines generated by (A) an rf electric field and (B) a dc trapping field in a field-corrected cell.

EXPERIMENTAL SECTION

All experiments were performed on a Texas A&M University (TAMU) two-section cell FT-ICR system. The system is equipped with an Oxford 3-T superconducting magnet and a Nicolet 1280 computer. In order to evaluate the effects of (i) reduction of the surface area of the receive electrodes and (ii) the use of guard rings, two different dual cell assemblies were constructed. Direct comparison of the different detectors (i.e., receive rods vis-a-vis receive plates) was accomplished by utilizing a two-section cell consisting of two cubic cells (3.81 × 3.81 × 3.81 cm) with a common center trap plate. The detection plates of one cell were replaced with receive electrodes comprised of oxygen-free copper rods (3 mm diameter). Comparisons between the field-corrected cell that incorporates guard rings and an orthorhombic ICR cell were made in dual cell assembly consisting of both ion cell assemblies. The two cells were mounted collinearly along the central axis of the magnetic field. The two cells share a common center trap plate comprised of a stainless steel mesh to ensure pressure conditions were the same in both regions. Ions were formed in all experiments by electron impact (50-eV electrons, 200 nA) using a rhenium ribbon filament. The vacuum system was maintained by 220 L/s oil diffusion pumps. Background pressures for both sections of the vacuum system were 1×10^{-8} Torr or less. Gaseous reagents were admitted to the detection regions by variable leak valves (Varian Series 951).

Inductance-Free Resistors. The voltage divider circuit between the shimming rings is produced by using noninductive resistors produced from Micronox resistive films. Use of noninductive resistors with rf circuits ensures linear resistance throughout the frequency range. The resistors used for the field-corrected cell (Caddock Electronics, Model No. MV261 10 Ω ± 0.01%) were bench tested and proven linear in the frequency range of dc–5.0 MHz with no propagation delay.

Excitation Waveform Generator. In the studies relating signal-to-noise ratio to cyclotron radius, ions of m/z 78 were accelerated by single frequency excitation allowing facile calculation of the resulting cyclotron radius. The excitation waveforms were created with a LeCroy Model 9100 arbitrary waveform generator (AFG). The waveforms are created by an IBM-AT computer using LeCroy EasyWave software. The output (50 Ω) of the AFG is set at 1.5 V (peak to peak) and the signal is further amplified by a broad-band amplifier which outputs the rf waveform to the FT-ICR cell. Manipulation of all waveform parameters required for the excitation (i.e., sweep rate, mass window, etc.) are directly controlled by software commands from the IBM computer.

Electrostatic Equipotential Plots. Electrostatic contours were calculated and displayed by using the trajectory calculation program SIMION (version 4.0) on a math coprocessor equipped PC/AT type IBM compatible computer. SIMION PC/PS2 V4.0 was developed by D. C. McGilvery and modified by D. A. Dahl. The program is distributed by D. A. Dahl, Idaho National Engineering Laboratory. SIMION allows placement of electrodes in a user-defined array permitting user-defined equipotential electric field lines to be calculated for the array. The potential array used for all calculations was 100,50 points (x,y in SIMION; z,y in FT-ICR conventions). SIMION allows for potential boundary conditions in only two perpendicular directions, so the ICR cell was generated by circular rotation of the potential array about the X axis. The remainder of the parameters were set at the default settings.

RESULTS AND DISCUSSION

The effect of reduced surface area must be evaluated in terms of the image current detected by the electrodes (i.e., signal sensitivity) and the production of harmonic signals in the frequency domain spectrum. The signal produced is proportional to the number of electric field lines produced by the ion packet which terminate on the surface of the receive plate. As illustrated in Figure 4A, the electric field lines generated by a charged ion packet terminate on the entire surface of the receive plate. The density of field lines terminating on the plate drops off as the square of the distance separating the ion packet from the plate. Reducing the area of the receive surface (Figure 4B) results in redirection of the field lines. Although some of the field lines generated by the cycloiding packet will terminate on the steel vacuum chamber surrounding the ion cell, it is reasonable to assume that there will be negligible loss due to the distance between the cell and the vacuum chamber. Because the same number of field lines terminate on the rod (through the capacitance bridge), there is *negligible loss* of sensitivity compared to a larger surface area. Furthermore, the same number of field lines terminating on a smaller area increases the induced charge per unit area. The signal voltage (RMS) detected in this manner is described by eq 3 (*27*, *28*), where V_s is the root mean square (RMS)

$$V_{s(\mathrm{RMS})} \propto (Nqr)/(dC) \qquad (3)$$

voltage detected, N and q are the number and charge on the ions, r and d are the radius of the cyclotron orbit and distance between the receive plates, and C is the capacitance. Since the area of the detector plate is directly proportional to the capacitance, a reduction of the area by replacing the receive plates with rods should yield an increase in the signal voltage detected.

Figure 5 is a plot of the signal-to-noise ratio for ions of m/z 78 (produced by electron impact ionization of benzene) de-

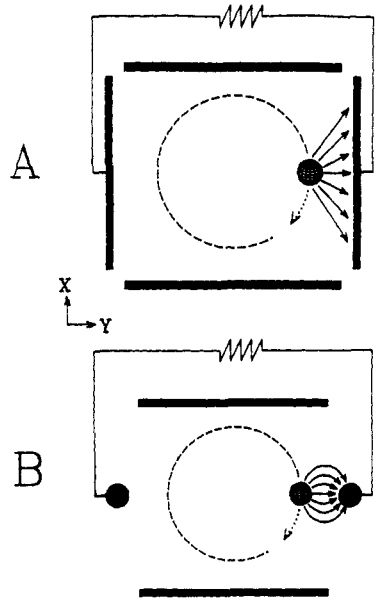

Figure 4. Electric field lines generated by a rotating ion packet. The same number of field lines terminate on both the plate (A) and rod (B) receive surfaces. Although some of the field lines generated by the cycloiding packet will terminate on the steel vacuum chamber surrounding the ion cell, it is reasonable to assume that there will be negligible loss of signal because of the distance between the cell and the vacuum chamber.

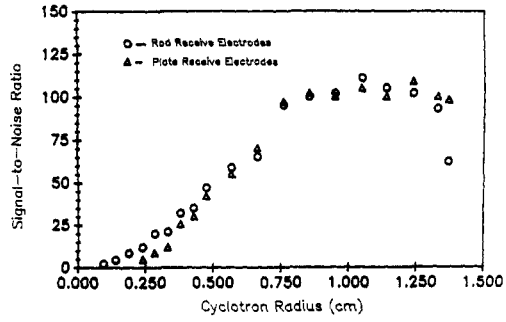

Figure 5. A plot of the signal-to-noise ratio for ions of m/z 78 as a function of radius. In this plot the relative sensitivity of receive rods vis-a-vis receive plates can be evaluated. The detected signal increases with radius resulting in an increase in the signal-to-noise ratio. It is important to note that at large cyclotron radii, the surface area of the receive plates had no effect on the signal-to-noise ratio.

tected by both plate surfaces and rod surfaces. The effect of reducing the receive surface area on detection can be investigated by comparing the signal-to-noise ratio as a function of cyclotron radius. Comparing signal-to-noise ratios as a function of cell geometry eliminates the effects of ion density differences between the two cells. Prior to excitation, the field lines produced by the random ion ensemble terminate equally on both receive surfaces resulting in common mode rejection and no detected signal. Upon excitation the ions are driven into coherence and a signal is detected. At small radii the signal detected is reduced by the produced field lines simultaneously interacting with both receive surfaces (resulting in common mode rejection) and the grounded excitation plates (resulting in loss of signal). The detected signal increases with radius resulting in an increase in the signal-to-noise ratio. It is important to note that at large cyclotron radii, the surface area of the receive plates had no effect on the signal-to-noise ratio. It can also be observed from Figure 5 that ion detection using receive rods was more sensitive to ions accelerated to small radii. This can be explained as a combination of both reduced surface area and an increased ability to drive ions into coherence. Both of these advantages result in increased performance in terms of initial ion detection.

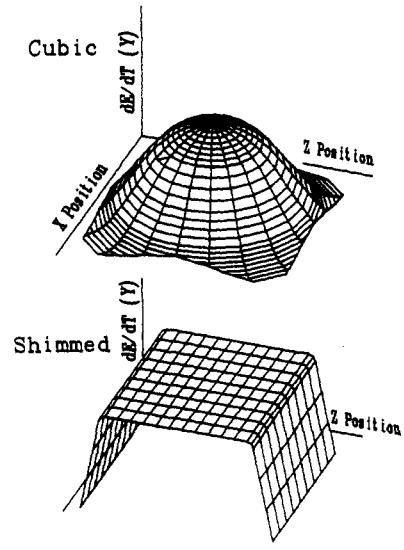

Figure 6. Plots of the rate at which energy is gained ($\delta E_k/\delta t$ from an rf electric field applied in the Y direction) as a function of ion position in the trap. Because of the field perturbations created by the trapping and receive plates during excitation, $\delta E_k/\delta t$ is strongly position dependent.

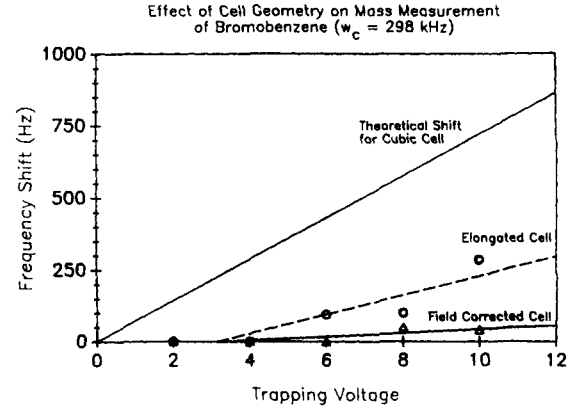

Figure 7. A plot of the shift in the observed frequency of bromobenzene (m/z 156, ω_c = 298 kHz) as a function of cell geometry.

By regulation of the voltages applied to the rings, the field lines are redirected to produce a field that is homogeneous (±1%) throughout ca. 95% of the dimensions of the ion cell. The increased homogeneity (X–Y plane) of the rf electric field enhances the uniform acceleration of the sample ions. Figure 6 contains plots of the rate an ion gains energy ($\delta E_k/\delta t$ from an rf electric field applied in the Y direction) as a function of ion position in the trap. Because of the field perturbations (cubic cell) created by the trapping and receive plates during excitation, $\delta E_k/\delta t$ is strongly position dependent and ions which are spatially distributed along the Z axis receive different amounts of translational energy during excitation. The excitation profile for the field-corrected cell is uniform throughout the dimensions of the detection region, thus $\delta E_k/\delta t$ is also uniform and *all* ions receive the same translational energy during excitation.

Figure 7 contains a plot of the shift in the observed cyclotron frequency of the bromobenzene molecular ions (m/z 156, ω_c = 298 kHz) using both cell geometries. From the plot it is clear that at higher trapping potentials the perpendicular component of the electric field increases causing shifts in the observed frequency. Note that the field-corrected cell effectively shields ion detection even at high trapping potentials.

Figure 8 contains the narrow-band mass spectrum of the bromobenzene molecular ion. A trapping voltage of 10 V was used for both the cubic and field-corrected ion cells. At high trap voltage, the peak shapes produced in a cubic ICR cell

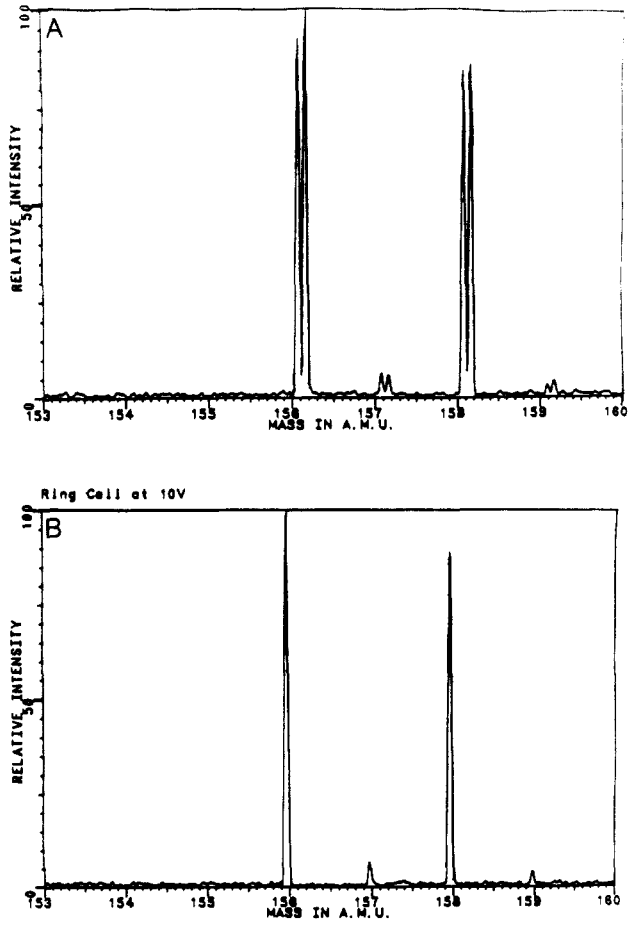

Figure 8. Narrow-band mass spectra of bromobenzene achieved at a trapping voltage of 10 V for (A) a cubic and (B) field-corrected ion cells.

are split into doublets. By reduction of the applied trapping field, a dramatic change in the peak shape is observed. Gross and Rempel have recently discussed the impact of high trapping field on peak shape and resolution (*29, 30*) and the signal-to-noise ratio was increased with corrected trapping fields (*31*).

Figure 9 contains a plot of the signal-to-noise ratio obtained for the cubic and field-corrected ICR cells. At low trapping potentials the signal-to-noise ratios are comparable (due to the limited **E** × **B** field interaction), but at high trapping voltages the applied electric field causes a significant loss in ion signal.

ALTERNATIVE CELL DESIGNS

Cell designs used for ion–molecule studies do not need to incorporate shimming rings to produce a narrow kinetic energy distribution. Recently we showed that a cell constructed of receive rods and hemispherical trap plates closely mimics the field-corrected cell. The use of hemispherical trapping electrode was first suggested by Smalley and co-workers (*32*), but when coupled with receive rods, it is possible to produce both homogeneous excitation and trapping fields in the detection region of the ion cell. Figure 10 contains a plot of equipotential lines produced in an ion cell using hemispherical trapping electrodes. The concave geometry redirects the field lines such that a linear trapping field is approximated in the detection region. Ions that are produced outside the detection region (i.e., within the concave region of the hemispherical trap plates) are lost from the cell during excitation and do not interfere with subsequent reaction studies. The low potential gradient within the detection region results in an initial kinetic energy distribution allowing accurate low-temperature reaction

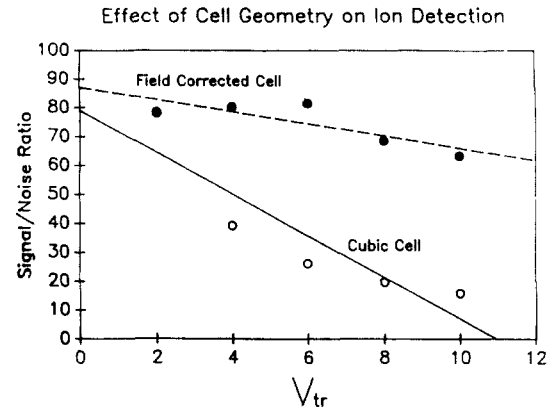

Figure 9. Plot of the signal-to-noise ratio obtained in the two ion cells. At low trapping potentials the signal-to-noise ratio is comparable due to the limited **E** × **B** field interaction. Conversely, at high trapping voltages the effects of the applied electric field cause a significant loss in detected ion signal resulting in a reduction of the signal-to-noise ratio.

to be observed similar to the field-corrected cell. The excitation field lines are also redirected (Figure 11A) along the Z axis resulting in near-homogeneous excitation in the detection region. Shown in Figure 11B is a plot of the equipotential lines generated in the $X-Y$ plane. Utilization of receive rods significantly reduces the radial inhomogeneities in the $X-Y$ plane created by the interaction of the rf electric field with large receive plates.

PRACTICAL ASPECTS OF OPTIMUM CELL DESIGN

The performance characteristics predicted for FT-ICR have been demonstrated under conditions where the ions are trapped in the cell with thermal kinetic energies. Although the potential utility of FT-ICR for high mass detection is indicated by the recent success in the detection of laser-desorbed organic molecules (*31*), the loss of mass resolution of high mass ions produced in an external ion source has not yet been solved (*33*). At m/z values greater than 2500 amu, the duration of the time-domain is insufficient for high-resolution measurements. Ions that are injected into an ion cell from an external source require high trapping voltage to capture the translationally hot ions. Because the ions are trapped with initially high translational energy, high excitation fields or long rf excitation periods are required to produce detectable packets of ions. In a cubic FT-ICR cell the application of high electric fields produces strong potential gradients that complicate both ion trapping and detection. Therefore, a field-corrected cell is of importance when attempting to reach the theoretical potential of FT-ICR in terms of high mass biomolecules.

It is important to note that the development of a cell which eliminates **E** × **B** field effects is equally suited for more conventional analytical application. The ability to produce and store a population of ions for extended periods of time makes FT-ICR an important technique for ion–molecule reaction studies. However, an important consideration of any energy-dependent reaction study is the initial kinetic energy distribution of the ion population. In a cubic FT-ICR cell, the initial kinetic energy distribution is determined by the trapping field. The translational energy acquired during the ionization event complicates kinetic studies. Furthermore, mass dependent Z-axis excitation and the effects of Z-axis motion in the presence of **E** × **B** fields reduces the ability to accurately monitor ion–molecule reactions. Shimming both the excitation and trapping electric fields permits ion detection and ion storage to occur in an electric field free region. Ion production in the confines of a low potential gradient results in a narrow kinetic energy distribution. A narrow initial

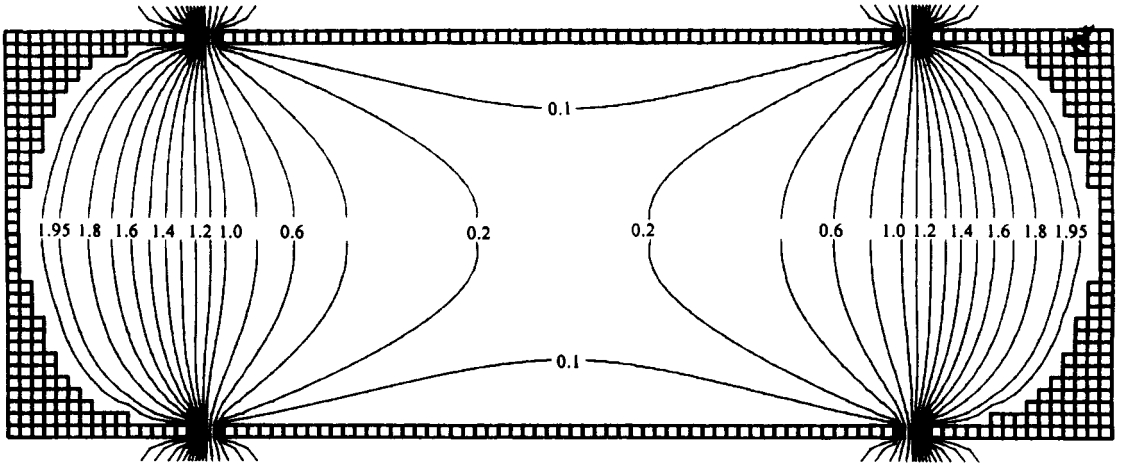

Figure 10. Plot of equipotential lines produced by using hemispherical trapping electrodes. The concave geometry redirects the field lines such that a linear trapping field is approximated by producing a high density of electric field lines which are perpendicular to the magnetic field. It is important to note the low potential gradient formed in the detection region of the cell relative to the potential gradient formed in a cubic ICR cell (Figure 1B).

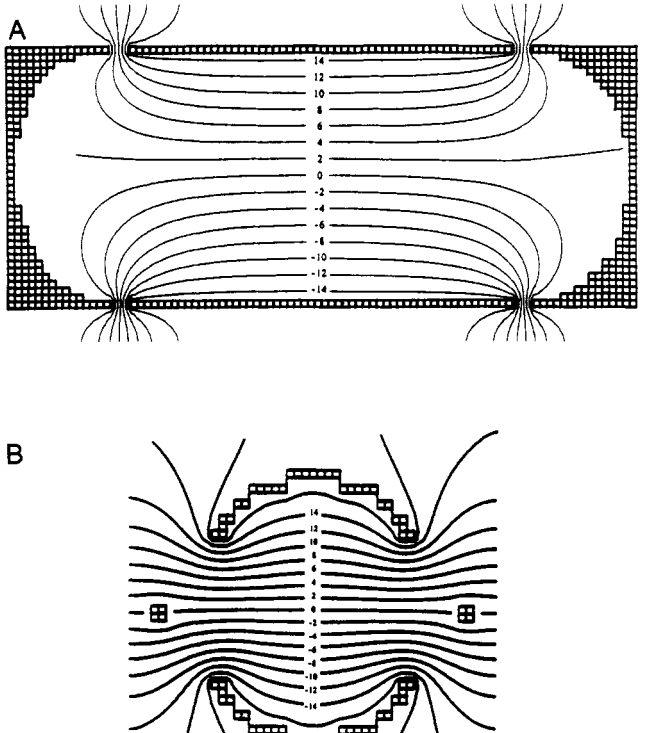

Figure 11. Plots of the equipotential lines generated in a cell constructed of hemispherical trapping plates in conjunction with receive rods and cylindrical excitation plates during excitation. A projection along the Z axis (A) shows that ions formed with low kinetic energies trapped in the center of the cell will experience uniform excitation. Ions that are formed at the extremes of the ion cell (and therefore acquire significant kinetic energies due to the high potential gradient) are discriminated against by the redirection of the field lines near the trap plates. A projection in the $X-Y$ plane (B) shows that uniform excitation can be achieved regardless of ion position.

kinetic energy distribution coupled with uniform excitation greatly improves the accuracy of ion–molecule reaction measurements.

Recently, we demonstrated that phase synchronization occurs via a frequency shift induced by an applied rf excitation. Phase synchronization and production of the coherent ion packet requires a uniform excitation field. The rf excitation electric field lines produced in a cubic FT-ICR cell are distorted by the detection plates which are held at ground during excitation. The inhomogeneities result in electric field vectors which are not uniformly applied in the Y direction. An rf electric field having a distribution of vector components in the X direction (i.e., radially inhomogeneous) causes misalignment of ions having initially different spatial locations and phase angles. Such differences in the alignments of the ions following excitation correspond to an inability to phase synchronize the ion population. In order to realize the potential of FT-ICR, modification of cell geometry to reduce the $\mathbf{E} \times \mathbf{B}$ field effects is necessary.

ACKNOWLEDGMENT

The authors wish to thank R. E. Smalley for his helpful discussions pertaining to the effect of field line termination on ion detection. We also gratefully acknowledge the many discussions with A. G. Marshall pertaining to the process and studies of novel cell designs.

LITERATURE CITED

(1) Comisarow, M. B.; Marshall, A. G. *J. Chem. Phys.* **1975**, *62*, 293.
(2) Marshall, A. G.; Comisarow, M. B. *Anal. Chem.* **1975**, *47*, 491A.
(3) White, R. L.; Ledford, E. B.; Ghaderi, S.; Wilkins, C. L.; Gross, M. L. *Anal. Chem.* **1980**, *52*, 1525.
(4) Alleman, M.; Kellerhals, Hp,; Wanczek, K. P. *Int. J. Mass Spectrom. Ion Processes* **1983**, *46*, 139.
(5) Ledford, E. B.; Ghaderi, S.; White, R. L.; Spencer, R. B.; Kulkarni, P. S.; Wilkins, C. L.; Gross, M. L. *Anal. Chem.* **1980**, *52*, 463.
(6) Ledford, E. B.; Remple, D. L.; Gross, M. L. *Anal. Chem.* **1984**, *56*, 2744.
(7) Schuch, D.; Chung, K. M.; Hartmann, H. *Int. J. Mass Spectrom. Ion Processes* **1984**, *56*, 109.
(8) Laukien, F. H. *Int. J. Mass Spectrom. Ion Processes* **1986**, *73*, 81.
(9) Kerley, E. L.; Castro, M. E.; Hanson, C. D.; Russell, D. H., submitted for publication in *Anal. Chem.*
(10) Sharp, T. E.; Eyler, J. R.; Li, E. *Int. J. Mass Spectrom. Ion Phys.* **1972**, *9*, 421.
(11) Dunbar, R. C. *Int. J. Mass Spectrom. Ion Processes* **1984**, *91*, 2801.
(12) Grese, R. P.; Rempel, D. L.; Gross, M. L. In *Fourier Transform Mass Spectrometry: Evolution, Innovation, and Applications*; Buchanan, M. V., Ed.; ACS Symposium Series 359; American Chemical Society: Washington, DC, pp 34–59.
(13) McIver, R. T. *Rev. Sci. Instrum.* **1970**, *41*, 555.
(14) Comisarow, M. B. *Int. J. Mass Spectrom. Ion Processes* **1981**, *37*, 251.
(15) Grosshans, P. B.; Wang, M.; Ricca, T. L.; Ledford, E. B.; Marshall, A. G. *Proceedings of the 36th Annual Conference on Mass Spectrometry and Allied Topics, San Francisco*; American Society for Mass Spectrometry: 1988, p 592.
(16) Hanson, C. D.; Castro, M. E.; Russell, Hunt, D. F.; Shabanowitz, J. In *Fourier Transform Mass Spectrometry: Evolution, Innovation, and Applications*; Buchanan, M. V., Ed.; ACS Symposium Series 359; American Chemical Society: Washington, DC, pp 100–115.
(17) Rempel, D. L.; Huang, S. K.; Gross, M. L. *Int. J. Mass Spectrom. Ion Processes* **1986**, *70*, 163.
(18) Kofel, P.; Allemann, M.; Kellerhals, Hp.; Wanczek, K. P. *Int. J. Mass Spectrom. Ion Processes* **1986**, *74*, 1.
(19) Huang, S. K.; Rempel, D. L.; Gross, M. L. *Int. J. Mass Spectrom. Ion Processes* **1986**, *72*, 15.
(20) Grese, R. P.; Rempel, D. L.; Gross, M. L. In *Fourier Transform Mass Spectrometry: Evolution, Innovation, and Applications*; Buchanan,

M. V., Ed.; ACS Symposium Series 359; American Chemical Society: Washington, DC, pp 34-59.
(21) Wang, M.; Marshall, A. G. *Anal. Chem.* **1989**, *61*, 1288.
(22) Wang, M.; Marshall, A. G. *Proceedings of the 36th Annual Conference on Mass Spectrometry and Allied Topics, Miami, FL*; American Society for Mass Spectrometry: 1989; RPA 9.
(23) Hanson, C. D.; Castro, M. E.; Russell, D. H. *Proceedings of the 37th Annual Conference on Mass Spectrometry and Allied Topics, Miami, FL*; American Society for Mass Spectrometry: 1989; RPA 34.
(24) Sommer, H.; Thomas, H. A.; Hipple, J. A. *Phys. Rev.* **1949**, *76*, 1877.
(25) Sommer, H.; Thomas, H. A.; Hipple, J. A. *Phys. Rev.* **1950**, *80*, 487.
(26) Sommer, H.; Thomas, H. A.; Hipple, J. A. *Phys. Rev.* **1951**, *82*, 697.
(27) Shockley, W. *J. Appl. Phys.* **1938**, *9*, 635.
(28) McIver, R. T.; Hunter, R. L.; Ledford, E. B.; Locke, M. J.; Francl, T. J. *Int. J. Mass Spectrom. Ion Processes* **1981**, *39*, 65.
(29) Remple, D. L. *Proceedings of the 35th Annual Conference on Mass Spectrometry and Allied Topics, Denver, CO*; American Society for Mass Spectrometry: 1987, p 1124.
(30) Remple, D. L.; Gross, M. L. *Proceedings of the 37th Annual Conference on Mass Spectrometry and Allied Topics, Miami, FL*; American Society for Mass Spectrometry: 1989; RPA 5.
(31) Ijames, C. F.; Wilkins, C. L. *J. Am. Chem. Soc.* **1988**, *110*, 2687.
(32) Smalley, R. E., Department of Chemistry, Rice University, Houston, Tx, private communication.
(33) Hunt, D. F.; Shabanowitz, J.; Yates, J. R.; Zhu, N.-Z.; Russell, D. H.; Castro, M. E. *Proc. Natl. Acad. Sci.* **1987**, *84*, 620.

RECEIVED for review August 8, 1989. Accepted November 27, 1989. This work was supported by the National Science Foundation (CHE-8418457). We gratefully acknowledge the Texas A&M University Office of University Research Services and the College of Science for providing a portion of the funds for purchase of the Nicolet FTMS 1000 mass spectrometer.

Combustion Tube Method for Measurement of Nitrogen Isotope Ratios Using Calcium Oxide for Total Removal of Carbon Dioxide and Water

Carol Kendall* and Elizabeth Grim

U.S. Geological Survey, 431 National Center, Reston, Virginia 22092

The nitrogen isotope ratios of several organic and inorganic materials have been analyzed by a sealed-tube combustion method requiring on-line cryogenic purification and by a new sealed-tube combustion technique using CaO for the quantitative removal of CO_2 and water. Samples purified cryogenically are enriched in ^{15}N by an average of 0.11‰ relative to samples prepared with CaO. The enriched values of samples purified cryogenically probably result from the larger amounts of residual contaminants in samples prepared without CaO. Because samples prepared with the CaO technique require no additional purification, the technique is ideal for use with multisample mass spectrometer inlet systems.

INTRODUCTION

In the years since Stump and Frazer (*1*) first proposed a dry combustion technique for the liberation of nitrogen, combustion techniques have become the preferred method for the analysis of organic and inorganic nitrogen samples for nitrogen isotopic composition. Most commonly, samples are combusted inside sealed tubes (*2*, *3*), the tubes are cracked into a vacuum line, the contents are purified cryogenically to remove H_2O and CO_2, sometimes further purified by cycling through various furnaces (*4*), and then the nitrogen gas is concentrated before introduction into the mass spectrometer or into a sample vessel by using a Toepler pump (*4*), by freezing with He (*5*, *6*), or by trapping onto a molecular sieve cooled by liquid nitrogen (*7-9*). The sample vessels may then be mounted on the mass spectrometer inlet system for isotope ratio measurement. Alternatively, samples may be combusted under vacuum in furnaces connected to the mass spectrometer and the purified gas frozen into a small inlet volume (*10*). All of these methods require considerable time and labor for the various purification and concentration steps. The recent availability of isotope ratio mass spectrometers equipped with multiple automated tube crackers makes sealed-tube techniques that produce pure gas especially attractive. Such techniques have been developed for preparation of water for δD determination (*11*).

In their classic papers, Fiedler and Proksch (*2*, *12*) describe their techniques and apparatus for the first multisample semiautomated inlet system for a nitrogen isotope ratio mass spectrometer. Their system enabled 80 samples to be processed per day. Samples were combusted in Pyrex tubes with copper and copper oxide, and CaO was added to absorb the resultant H_2O, CO_2, HCl, and other products. The low reaction temperature required by Pyrex produced incomplete yields (85-90%), which impaired precision and accuracy, making the technique unsuitable for natural abundance measurements. The authors rejected the use of quartz tubes because of cost, because of difficulty of handling, and because they found that quartz reacted with CaO at temperatures above 600 °C and cracked due to formation of calcium silicates. We have combined their use of CaO with our current 850 °C sealed-tube technique, which is modified after Macko (*8*), and have experienced no problem with reaction of CaO with Vycor tubes. The use of CaO results in complete removal of CO_2 and H_2O and, hence, is ideal for use with a multiport tube-cracking inlet system.

This study compares our former and new sealed-tube combustion techniques for precision, accuracy, and ease of use. Samples prepared by either method are cracked directly into the inlet system of the mass spectrometer. However, samples prepared without CaO require cryogenic purification on-line prior to analysis, whereas samples prepared with CaO may be directly introduced into the mass spectrometer without further purification.

EXPERIMENTAL SECTION

Apparatus. Samples are combusted in 9-mm Vycor tubes inside hollow nickel tubes in a muffle oven. The nickel tubes protect adjacent tubes from exploding if one tube explodes. After combustion, a custom-made temperature controller cools the samples for 17 h by automatically decreasing the temperature at